

**PROJECT #2015-008**

DATE: April 17, 2015

# **In-Situ Performance Verification of Geogrid-Stabilized Aggregate Layer: West Hunt Highway, San Tan Valley, AZ**

By

David J. White, Ph.D., P.E.

*Ingios Geotechnics, Inc.*



Prepared for Tensar International Corporation, Alpharetta, GA

---

## Executive Summary

At the request of Tensar Corporation, Ingios Geotechnics, Inc. conducted automated plate load tests (APLTs) on West Hunt Highway in San Tan Valley, AZ. Seven cyclic APLTs and one confining-stress dependent cyclic APLT were conducted to determine in-situ resilient modulus ( $M_r$ ), and one static APLT each was conducted to determine modulus of subgrade reaction ( $k$ ) per AASHTO T-222 and strain modulus ( $E_v$ ) per DIN 18134 (2001). The focus of the testing program was to evaluate the pavement foundation comprising uncrushed aggregate base roadway stabilized with TX5 multi-axial geogrid with hexagonal structure and triangular apertures. Tests were performed on April 17, 2015.

In-situ testing involved performing 1,000 cycle APLT tests using a 12 in. diameter plate. The stresses selected for the cyclic tests were 2 psi to 50 psi (cyclic stress difference of 48 psi). Plate deflections were monitored and a sensor kit was installed to measure ground deflections at selected radial distances (2 x and 3 x plate radius) from the plate center. At each of the APLT test locations, a dynamic cone penetration (DCP) test was performed to determine the penetration resistance profile up to about 2.5 ft below the surface. The base layer was excavated by hand to determine the thickness of the base layer for layered analysis. The aggregate base course layer was 5.4 in. thick on average. The aggregate base course classified as poorly-graded gravel with sand and silt (GP-GM) with a 5.7% fines content

The average in-situ composite resilient modulus in the TX5 geogrid stabilized section was about 34,251 psi after 1,000 load cycles for the applied 48psi cyclic stress. The layered analysis in-situ resilient modulus averaged 155,694 psi for the aggregate base layer and 16,144 psi for the subgrade layer. Of the seven layered analysis tests, two tests did not meet the analysis criteria for the equivalent thickness to plate radius ratio of greater than 1. These two tests produced low resilient deflections at the 2r and 3r sensor positions that is characteristic of dilatancy in the unconfined aggregate outside of the perimeter of the loading plate.

For the 10,000 cycle test, the in-situ resilient modulus increased rapidly in the aggregate base layer for the first ~3000 cycles and then continued to increase at a slower rate. Based on a permanent deformation rate of 0.0001

in./cycle, the transition from plastic deformation accumulation to near-linear elastic behavior ( $N^*$ ) occurred at 8,696 load cycles. At  $N^*$ , the in-situ  $M_r$  of the aggregate base layer was about 321,881 psi (2 times higher than the average value from the at 1,000 cycle tests).

From the static plate load tests it was determined that the  $E_{v1}$  was 13,689 psi with an  $E_{v2}/E_{v1}$  ratio of 1.60. These values meet or exceed the European specified limits for top aggregate base layer. The modulus of subgrade reaction,  $k_u$ , was 392 pci as measured from the 30 in. diameter plate.

Permanent deformations were observed to increase at a near-linear rate with increasing load cycles for some of the 1,000 cycle tests and the 10,000 cycle test. Previous experience with 10,000 cycle testing with more well-graded aggregates at other sites indicate permanent deformation plots that are less linear (more asymptotic). This near-linear trend is presumably linked to the frictional characteristics of the aggregate particles and number of grain contacts.

A cyclic confining stress-dependent resilient modulus test was performed to determine the relationship between stress and modulus. The model parameters show that as the maximum cyclic stress decreases, the in-situ resilient modulus increases. For this project a 1 psi surface confinement with 15 psi maximum cyclic stress results in  $M'_{r,\sigma} = 69,207$  psi.

Observation of the resilient deflections with loading cycles show that the TX5 stabilized aggregate base becomes more resilient with increasing loading cycles beyond about 100 cycles.

**DISCLAIMER:**

Ingios Geotechnics, Inc. and its Affiliates disclaim any and all responsibility and liability for the use of any such data, information and/or the analysis presented in this report. Although Ingios Geotechnics, Inc. takes all possible care to ensure the correctness of published information, no warranty can be accepted regarding the correctness, accuracy, uptodateness, reliability and completeness of the content of this information.

Ingios Geotechnics, Inc. expressly reserves the right to change, to delete or temporarily not to publish the contents wholly or partly at any time and without giving notice. Liability claims against Ingios Geotechnics, Inc. because of tangible or intangible damage arising from accessing, using or not using the published information, through misuse of the contents or as a result of technical breakdowns are excluded.

# Contents

Executive Summary .....	ii
<b>1 Introduction .....</b>	<b>1</b>
1.1 Background .....	1
1.2 Objective .....	2
1.3 Scope.....	2
<b>2 Test Methods.....</b>	<b>3</b>
2.1 Automated Plate Load Test (APLT) .....	3
2.1.1 <i>Composite Resilient Modulus</i> .....	5
2.1.2 <i>Layered Analysis</i> .....	8
2.1.3 <i>Permanent Deformation Monitoring</i> .....	10
2.1.4 <i>E<sub>v</sub> Strain Modulus Testing</i> .....	10
2.1.5 <i>Modulus of Subgrade Reaction Testing</i> .....	13
2.1.6 <i>Confining Stress-Dependent Resilient Modulus Test</i> .....	14
2.2 Dynamic Cone Penetration (DCP) Testing .....	16
2.3 Laboratory Testing.....	16
<b>3 Experimental Study .....</b>	<b>17</b>
3.1 Field Experimental Study.....	17
3.2 Project Details .....	18
<b>4 Results.....</b>	<b>23</b>
4.1 Dynamic Cone Penetration (DCP) Test Results.....	23
4.2 In-Situ Composite Resilient Modulus .....	24
4.3 Two-Layer In-situ Resilient Modulus .....	25
4.4 E <sub>v</sub> Strain Modulus.....	29
4.5 Modulus of Subgrade Reaction, <i>k</i> -value .....	29
4.6 In-situ Confining Stress Dependent Modulus .....	30
4.7 Predicting Trafficking Performance.....	31
4.8 Additional Findings.....	34
<b>5 Conclusions and Recommendations .....</b>	<b>36</b>
References .....	38

## Figures

Figure 1. APLT test system.....	4
Figure 2. Example output from APLT test system.....	4
Figure 3. APLT test setup with deformation measurements obtained at $2r$ and $3r$ from the plate center axis. ....	6
Figure 4. Illustration of Odemark’s MET concept. ....	9
Figure 5. APLT test setup with 30 in. diameter plate for AASHTO T222 static plate load test (note: wheels not in contact with ground during testing).....	14
Figure 6. APLT test setup with a confining plate and a 8 in. diameter loading plate. ....	15
Figure 7. APLT test locations on April 17, 2015 testing between N. Mountain Vista Blvd & N. Village Lane in San Tan Valley, AZ. ....	18
Figure 8. Aggregate base course over TX5 (April 17, 2015).....	19
Figure 9. Pneumatic tired roller used just prior to testing (April 17, 2015). ....	20
Figure 10. APLT testing at 30 in. static test point (April 17, 2015). ....	20
Figure 11. (top) Full gradation sample and (bottom) aggregate base course retained on No. 4 sieve after washing and oven-drying (April 17, 2015 sample).....	21
Figure 12. Grain-size analysis and classification of aggregate base course material with limits shown for MAG (2013) Standard Specification Section 310 (sampled April 17, 2015). ....	22
Figure 13. DCP profiles for all test locations.....	23
Figure 14. Summary of aggregate layer thicknesses and in-situ measurement values.....	25
Figure 15. Comparison of permanent plate deformation and resilient deflections at 1,000 at points 1 to 7 and 10,000 cycles at point 4.....	26
Figure 16. Permanent plate deformation and resilient deflections measured at the edge of the plate and at $2r$ and $3r$ away from the plate center at test point 4 with 10,000 cycles. ....	27
Figure 17. In-situ $M_r$ of base and subgrade layers from layered analysis versus number of cycles at test point 4 with 10,000 cycles.....	28
Figure 18. $E_v$ strain modulus applied stress versus settlement for TX5 section. ....	29
Figure 19. k-value modulus of subgrade reaction for 30 in. diameter static plate load test for TX5 section. ....	30
Figure 20. In-situ $M_{r,\sigma}$ model and permanent deformation results for TX5 section. ....	31
Figure 21. Permanent deformation versus load cycle number at all test points.....	33
Figure 22. Resilient deflection versus load cycle number for all test points. ....	34
Figure 23. Change in resilient deflection (relative to the minimum resilient deflection) versus load cycle number for all test points.....	35



---

## Tables

Table 1. Summary of target $E_{v1}$ values per ISSMGE (2005) specifications. ....	12
Table 2. Summary of target $E_{v2}$ and $E_{v2}/E_{v1}$ ratio values per (ATB Vag 2005) – English units. ....	12
Table 3. Summary of target $E_{v2}$ and $E_{v2}/E_{v1}$ ratio values per (ATB Vag 2005) – Metric units. ....	13
Table 4. Example confining stress-dependent resilient modulus test sequence. ....	15
Table 5. Summary of plate tests and configurations. ....	17
Table 6. Summary geogrid material mechanical properties. ....	17
Table 7. Summary of project location and notes. ....	18
Table 8. Comparison of test results for in-situ $M'_r$ and permanent deformation April 17, 2015 in-situ testing. ....	24
Table 9. Summary of permanent deformation prediction parameters ....	32



---

# 1 Introduction

## 1.1 Background

The static plate load test (AASHTO T222) has been widely used in different geotechnical engineering fields and particularly in the characterization of foundation layer properties for rigid pavements. The strain or deformation modulus ( $E_v$ ) is commonly used in pavement design in Europe, while the resilient modulus is used in the U.S. The strain modulus,  $E_{v2}$  is calculated from the second loading cycle using the Boussinesq solution and secant method (DIN 18134, 2001). In contrast, resilient modulus ( $M_r$ ) is determined using *resilient* deflection of materials after many stress cycles. Resilient modulus can be obtained from the laboratory triaxial test (e.g., per AASHTO T307, 2000 or NCHRP, 2004). However, due to the complexity of the laboratory triaxial test and often non-representative boundary conditions, the resilient modulus of pavement foundation materials is often obtained from empirical correlations between resilient modulus and other properties such as soil classification, California Bearing Ratio (CBR) or Hveem R-value.

In-situ resilient modulus is also predicted from non-destructive surrogate tests including the falling weight deflectometer (FWD) or light weight deflectometer (LWD). In practice, elastic moduli values calculated from these test devices based on *elastic* deformations are often confused with resilient modulus values which is based on *resilient* (i.e., recoverable) deformations.

One of the major limitations of these non-destructive surrogate tests is the lack of a conditioning stage prior to testing. During pavement construction, pavement foundation materials are subject to relatively high loads from construction traffic and compaction equipment. In response to these loads, aggregate particles rearrange themselves resulting in higher density and stiffness. For mechanically stabilized layers, this results in greater interlock and aggregate confinement. For this reason, it is important to apply conditioning load cycles prior to testing to determine in-situ resilient modulus. Once surface paving is complete, the pavement foundation below is confined by the overlying pavement layers. The response of a pavement foundation to subsequent repeated traffic loading is both nonlinear and stress-dependent and therefore the effect of confinement is an important

---

condition to consider in a field based resilient modulus test. In response to this need, the Automated Plate Load Test (APLT) system was designed to directly measure the influence of load cycles and confining pressure on in-situ resilient modulus and permanent deformation of the pavement foundation.

## 1.2 Objective

The objective of this study was to conduct cyclic APLTs to determine in-situ  $M_r$  and deformation characteristics, and static APLTs to determine modulus of subgrade reaction ( $k$ ) and  $E_v$  strain modulus of the mechanically stabilized aggregate base and subgrade foundation layers. The road test section consisted of aggregate layers stabilized using TX5 multi-axial geogrid with hexagonal structure and triangular apertures.

## 1.3 Scope

Cyclic APLTs with up to 1,000 cycles were performed at seven test locations and 10,000 cycles at one test location using a 12 inch diameter plate, including a sensor kit to measure ground deflections at selected radial distances from the plate center. The cyclic test results were used to determine composite, stabilized base, and subgrade layer  $M_r$  values. In addition, one cyclic APLT with controlled confining and cyclic stresses similar to the AASHTO T307 (2000) was conducted, using an 8 in. inch diameter loading plate and a 24 in. diameter confining plate around the loading plate, to develop a stress-dependent constitutive model to predict in-situ  $M_r$ .

Static APLTs were performed at two locations, with one test conducted in accordance with AASHTO T222 to determine  $k$  and another test in accordance with DIN 18134 (2001) to determine  $E_v$  values.

Dynamic cone penetration tests (unconfined surface) were performed at each cyclic APLT test location to determine penetration resistance and California bearing ratio of profiles up to a depth of about 2.5 ft below surface. Photographs documented the surface conditions. Results were used to evaluate performance of the TX5 road section.

---

## 2 Test Methods

### 2.1 Automated Plate Load Test (APLT)

For rapid field assessment of critical performance parameters, Automated Plate Load Test (APLT) equipment was developed by Dr. David J. White (U.S. and International Patents Pending). The APLT equipment was specifically developed to perform rapid field testing of pavement foundations, embankments, stabilized materials. The APLT equipment is capable of measuring the following:

- Modulus of subgrade reaction
- Confining stress dependent resilient modulus
- Strain modulus
- Permanent deformation
- Bearing capacity
- Undisturbed tube sampling and extrusion
- Shear wave velocity/modulus
- Cone penetration testing
- Borehole shear testing
- Rapid in-situ permeability

Figure 1 shows the plate load test equipment mounted on a trailer unit and Figure 2 is an example of the data out-put including the stress cycles, cyclic and permanent deformation, stress-displacement relationship, number of load cycles, and in-situ resilient modulus. The APLT unit is automated using electric-hydraulic control systems.



Figure 1. APLT test system.

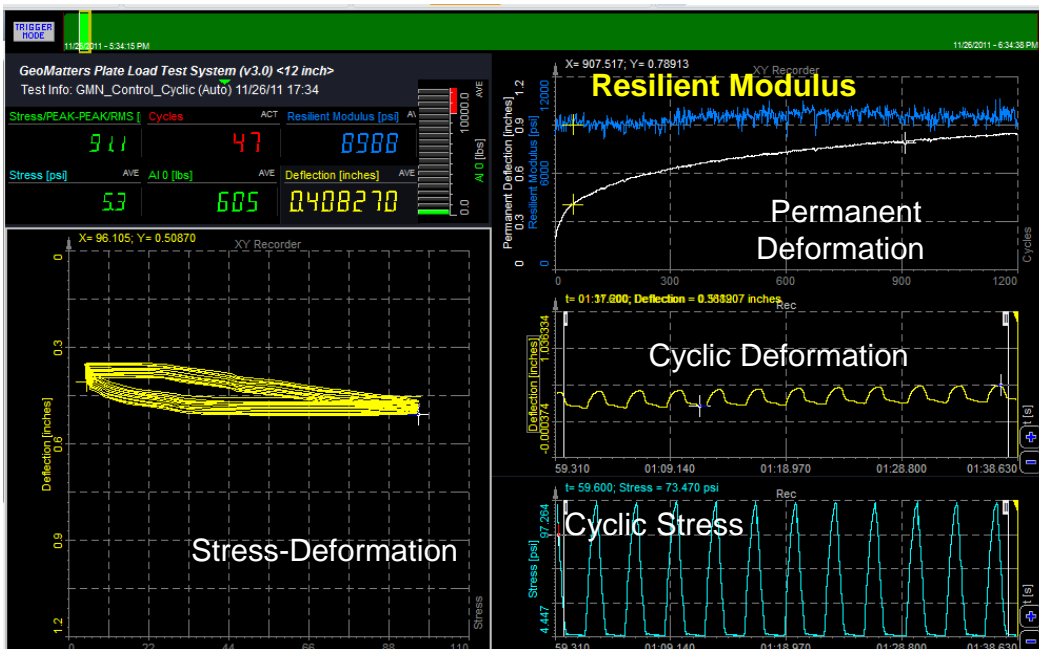


Figure 2. Example output from APLT test system.

### 2.1.1.1 Composite Resilient Modulus

The in-situ composite  $M_r$  was calculated as the ratio of the cyclic stress divided by the resilient deflection (during unloading) using the Boussinesq's half-space equation:

$$M_r = \frac{(1-\nu^2) \cdot \Delta\sigma_p \cdot r}{\delta_r} \times f \quad (1)$$

where,

$M_r$  is in-situ composite resilient modulus (uncorrected),

$\delta_r$  is the resilient deflection of plate during the unloading portion of the cycle (determined as the average of three measurements along the plate edge, i.e., at a radial distance  $r' = r$ ),

$\nu$  is the Poisson ratio (assumed as 0.40),

$\Delta\sigma_p$  is the cyclic stress,

$r$  is the radius of the plate,

$f$  is the shape factor selected as 8/3 for rigid plate on granular material.

In reality, Poisson's ratio will vary between test sections due to the aggregate stabilization mechanism(s) and loading conditions. Several papers in the literature demonstrate that this value can vary from 0.1 to 1+ due to the stress level and volume change characteristics (e.g., Brown et al. 1975, LeKarp et al. 2000).

Corrections to the measured in-situ composite  $M_r$  can be made as shown in Eq. (2) for plate bending ( $F_{Bending}$ ), plate size ( $F_{PlateSize}$ ), and the effect of future saturation ( $F_{Saturation}$ ) in the subgrade:

$$M'_r = \frac{(1-\nu^2) \cdot \Delta\sigma_p \cdot r}{\delta_r} \times f \times F_{Bending} \times F_{PlateSize} \times F_{Saturation} \quad (2)$$

In this report, no corrections were made for plate bending (i.e.,  $F_{Bending}$  is assumed as 1). The 8 inch diameter plate was approximately 5 in. thick and the 12 inch diameter plate was 1 in. thick with a 6 in. diameter plate that is 1 in. thick and a carriage plate as shown in Figure 3. Further, no corrections were applied for future saturation conditions (i.e.,  $F_{Saturation}$  is 1).

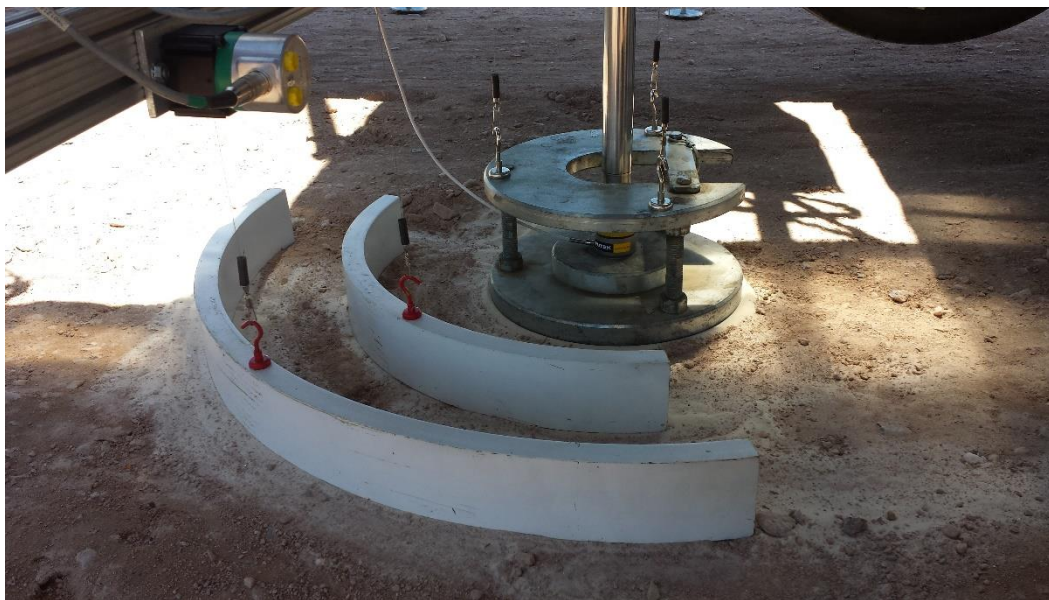


**Figure 3. APLT test setup with deformation measurements obtained at  $2r$  and  $3r$  from the plate center axis.**

Plate size corrections are often considered in field evaluations as the influence depths change with different plate sizes (typically assumed as twice the plate diameter). There is also a scale effect that is a function of the plate circumference to plate area ratio.

According to ASTM D1195-93 (2004) and AASHTO T221-90 (2012) for repetitive static plate load tests of soil and flexible pavement components:

*“...For evaluation purposes alone, a single plate may be used, provided that its area is equal to the tire-contact area corresponding to what may be considered as the most critical combination of conditions of wheel load and tire pressure. For the purpose of providing data indicative of bearing index (for example, the determination of relative subgrade support throughout a period of a year), a single plate of any selected size may be used”.*

Thus no requirement is specified for plate size correction, just that the plate size match the tire-contact area and pressure and that the same plate size be used for comparative analysis. Herein the 12 in. diameter plate was selected as the critical reference size and therefore the 8 in. diameter plate tests were corrected to a 12 inch diameter equivalent.

Correction factors can be determined experimentally, but are commonly based on Terzaghi's empirical equations (Terzaghi 1955) to estimate modulus of subgrade reaction ( $k$ ) values for different footing sizes from plate load test:

$$k_s = \frac{B_1}{B} \times k_1 \quad (\text{for footings on clay}) \quad (3)$$

$$k_s = \left( \frac{B + B_1}{2B} \right)^2 \times k_1 \quad (\text{for footings on sand}) \quad (4)$$

where,

$B_1$  = side dimension of a square plate used in load test or diameter of a circular plate (in.);

$B$  = width of footing for a square plate and diameter of footing if circular (in.), in this case = 12 inches;

$k_1$  = modulus of subgrade reaction from plate load test with plate size  $B_1$  (psi/in); and

$k_s$  = corrected modulus of subgrade reaction for the footing size (psi/in).

Ingios Geotechnics, Inc. evaluated plate size correction factors for cyclic testing as a function of cyclic stress for 6 in., 8 in., 10 in., 12 in., 18 in., 24 in., and 30 in. diameter plates on geogrid stabilized aggregate base layer over relatively soft subgrade (White, 2015). The results indicated that composite  $M_r$  values were not influenced by plate diameters  $\geq 12$  in. at two different cyclic stress levels (9 and 18 psi). Correction factors of 0.78 (for 9 psi cyclic stress) and 0.71 (for 18 psi cyclic stress) were determined to convert in-situ composite  $M_r$  for an 8 in. plate to the 12 in. diameter plate. Additional efforts are underway to quantify these correction factors for different composite and stiffness conditions.

In this report, the plate size correction was conservatively determined using an average of Eqs. (3) and (4) for tests on the composite aggregate base layers over subgrade,  $F_{PlateSize} = 0.68$  to convert the 8 in. diameter plate results to 12 in. diameter equivalent.

### 2.1.2 Layered Analysis

Individual subgrade and base layer resilient modulus values were determined by obtaining resilient deflections measured at radii of 12 in. ( $2r$ ), and 18 in. ( $3r$ ) away from the plate center. The test setup is shown in Figure 3. The layered analysis measurement system was developed specifically for testing of unbound materials and provides average resilient deflections measured over one-third of the circumference of a circle at the selected radii. This method was designed to improve upon practices that use point measurements, which are often variable from point-to-point for unbound aggregate materials.

Eq. (5) as suggested by AASHTO (1993) can be used to determine subgrade layer resilient modulus value:

$$M_{r(sg)} = \frac{(1 - \nu^2) \cdot P}{\pi \cdot r' \cdot \delta_{r,r'}} \quad (5)$$

where,

$M_{r(sg)}$  is in-situ subgrade resilient modulus (psi),

$\delta_{r,r'}$  is the resilient deflection (in.) during the unloading portion of the cycle at  $r' = 2r$  or  $3r$  away from plate center,

$\nu$  is the Poisson ratio (assumed as 0.40),

P is the cyclic load (lbs),

Ullidtz (1987) described Odemark's method of equivalent thickness (MET) concept, as illustrated in Figure 4, which shows a two-layered system on the left part with different moduli values for each layer.  $M_{r1}$  represents the resilient modulus of the top layer,  $M_{r2}$  represents the resilient modulus of the bottom layer, and  $h$  represents the thickness of the top layer. The Odemark's MET concept is that the top layer is transformed into a layer of equivalent thickness  $h_e$  with properties of the bottom layer (Ullidtz 1987). The  $h_e$  is calculated using Eq. (6), which can be simplified to Eq. (7), if Poisson's ratio ( $\nu$ ) is assumed as the same for the two layers:

$$h_e = h \times \sqrt[3]{\frac{M_{r1}(1 - \nu_1^2)}{M_{r2}(1 - \nu_2^2)}} \quad (6)$$



$$h_e = h \times 3 \sqrt{\frac{M_{r1}}{M_{r2}}} \quad (7)$$

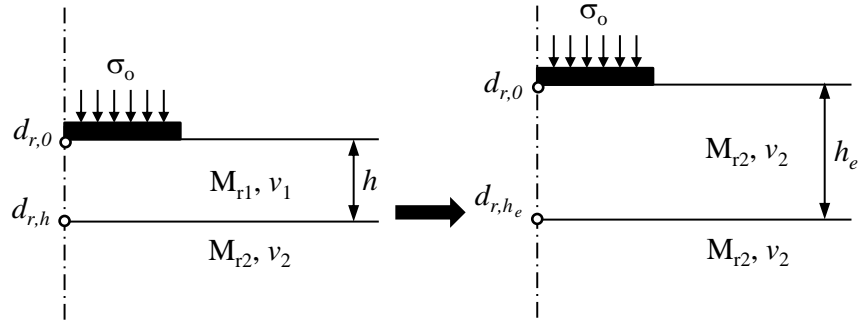


**Figure 4. Illustration of Odemark's MET concept.**

Using the Boussinesq's solution for linear-elastic materials and Odemark's MET method, Eq. (8) from AASHTO (1993) can be solved to determine the resilient modulus of the base layer ( $M_{r(base)}$ ):

$$\delta_c = (1 - \nu^2) \sigma_o r f \left[ \frac{1}{M_{r(sg)} \sqrt{1 + \left( \frac{h}{r} \times 3 \sqrt{\frac{M_{r(base)}(1 - \nu_1^2)}{M_{r(sg)}(1 - \nu_2^2)}} \right)^2}} + \frac{\left( 1 - \frac{1}{\sqrt{1 + \left( \frac{h}{r} \right)^2}} \right)}{M_{r(base)}} \right] \quad (8)$$

where,

$\nu_1$  and  $\nu_2$  are Poisson ratio's for base and subgrade layer, respectively (assumed as 0.40 for both), and

$h$  is the thickness of the base layer (in.).

Past research has shown that stress measurements in two-layer systems of aggregate base over compressible subgrade are very similar to those predicted by Boussinesq's analysis (e.g., McMahon and Yoder, 1960; Sowers and Vesic, 1961).

The two-layered analysis using the Odemark method is applicable for conditions with moduli values decreasing with depth (i.e., hard over soft), preferably by a factor of at least two between the consecutive layers (Ullidtz 1987). Ullidtz (1987) also noted that the  $h_e$  should be larger than the radius of the loading plate, i.e.,  $h_e/r > 1$ .

### 2.1.3 *Permanent Deformation Monitoring*

Permanent deformation results from cumulative plastic shear strain, compaction, and consolidation during loading. Permanent deformation ( $\delta_p$ ) was monitored during cyclic plate load testing. From the number of load cycles ( $N$ ) versus  $\delta_p$  plot, a deformation performance prediction model was developed to analyze and forecast the number of cycles to achieve a selected permanent deformation in the foundation layers. A power model was selected to represent the permanent deformation versus number of cycles as shown in Eq. 11:

$$\delta_p = CN^d \quad (11)$$

where, coefficient  $C$  is the plastic deformation after the first cycle of repeated loading, and  $d$  is the scaling exponent.

Monismith et al. (1975) described a similar power model relationship for relating permanent strain to cycle loadings for repeated triaxial laboratory testing. It is expected that  $C$  depends on the soil type, soil physical state, and stress conditions (See Li and Selig 1994) and  $d$  is expected to be relatively independent of these factors including resilient deflection.

The rate change of the permanent deformation is used herein to estimate the post-compaction permanent deformation and the corresponding number of loading cycles. Post-compaction permanent strain is a function of the shear stress magnitude and can reach an equilibrium state following the “shakedown” concept (see Dawson and Feller, 1999).

### 2.1.4 *$E_v$ Strain Modulus Testing*

The DIN 18134 (2001) standard for plate load test describes the procedure to calculate strain moduli ( $E_v$ ) values using different plate sizes. In this study, the plate load test was conducted using a 12 in. diameter plate (305 mm).

The test involves three steps: (1) preloading, (2) first loading cycle, and (3) second loading cycle. In the first step, the test area is preloaded at a normal stress of about 1.5 psi (0.01 MPa) for about 30 seconds and the load and settlement gauges are zeroed. In the second and third steps, the loading is applied in at least six steps with approximately equal increments, until the maximum normal stress is achieved. Each loading stage is completed within 1 minute and the load is maintained for about 1 minute for testing on base layers and for about 2 minutes for testing on subgrade layers. The unloading is performed by decreasing the load to 50% and 25% of the maximum normal stress. For a 12 in. diameter plate, the load is increased until a settlement of 0.20 in (5 mm) or a normal stress of 72.5 psi (0.5 MPa), whichever occurs first, is achieved. If a higher load than intended is inadvertently applied, it is specified that it must be noted in the testing records.

The strain modulus for first loading cycle ( $E_{v1}$ ) and for second loading cycle ( $E_{v2}$ ) is determined from a smooth applied stress vs. settlement curve. A second-order polynomial (quadratic) fit is applied to each loading cycle separately, using Eq. (12):

$$s = a_0 + a_1\sigma_0 + a_2\sigma_0^2 \quad (12)$$

where  $a_0$ ,  $a_1$ ,  $a_2$  are regression coefficients,  $s$  = settlement, and  $\sigma_0$  = applied stress. For the first loading cycle, data at  $s = 0$  is ignored.  $E_v$  values (in units of psi) are determined from Eq. (13):

$$E_v = 1.5 \cdot r \times \frac{1}{a_1 + a_2\sigma_{o\max}} \quad (13)$$

where  $r$  = radius of plate (in.) and  $\sigma_{o\max}$  = maximum applied stress (psi).

For reference, Tables 1 to 3 summarize target  $E_v$  values used in Europe for quality assurance of different layers or depths below the top of base.

**Table 1. Summary of target  $E_{v1}$  values per ISSMGE (2005) specifications.**

Test Depth	$E_{v1}$ , MPa	$E_{v1}$ , ksi
1 m (3.3 ft) below subgrade	15 (cohesive)	2.18 (cohesive)
	20 (cohesionless)	2.90 (cohesionless)
Top of subgrade	25 (cohesive)	3.63 (cohesive)
	35 (cohesionless)	5.08 (cohesionless)
Top of subbase	60 (rounded aggregate)	8.70 (rounded aggregate)
	72 (angular aggregate)	10.44 (angular aggregate)
Top of base	75 (rounded aggregate)	10.88 (rounded aggregate)
	90 (angular aggregate)	13.05 (angular aggregate)

**Table 2. Summary of target  $E_{v2}$  and  $E_{v2}/E_{v1}$  ratio values per (ATB Vag 2005) – English units.**

Depth below surface of base layer (inches)	Asphalt Pavement				Concrete Pavement			
	N	Min. $E_{v2}$ (ksi)	Avg. $E_{v2}$ (ksi)	Ratio* $E_{v2}/E_{v1}$	N	Min. $E_{v2}$ (ksi)	Avg. $E_{v2}$ (ksi)	Ratio* $E_{v2}/E_{v1}$
0-10 in.	8	18.13	$\geq 20.31+0.96\sigma$	$\leq 2.8$	8	15.23	$\geq 17.40+0.96\sigma$	$\leq 2.8$
0-10 in.	5	18.13	$\geq 20.31+0.83\sigma$	$\leq 1 + 0.013E_{v2}$	5	15.23	$\geq 17.40+0.83\sigma$	$\leq 1 + 0.015E_{v2}$
10-20 in.	8	4.64	$\geq 5.80+0.96\sigma$	$\leq 2.8$	8	6.53	$\geq 7.98+0.96\sigma$	$\leq 3.5$
10-20 in.	5	4.64	$\geq 5.80+0.83\sigma$	$\leq 1 + 0.063E_{v2}$	5	6.53	$\geq 7.98+0.83\sigma$	$\leq 1 + 0.046E_{v2}$
20 to 21.7 in.	8	4.64	$\geq 5.80+0.96\sigma$	NA	8	6.53	$\geq 7.98+0.96\sigma$	NA
20 to 21.7 in.	5	4.64	$\geq 5.80+0.83\sigma$	NA	5	6.53	$\geq 7.98+0.83\sigma$	NA
21.7 to 25.6 in.	8	2.90	$\geq 5.80+0.96\sigma$	NA	8	4.35	$\geq 5.08+0.96\sigma$	NA
21.7 to 25.6 in.	5	2.90	$\geq 5.80+0.83\sigma$	NA	5	4.35	$\geq 5.08+0.83\sigma$	NA
25.6 to 29.5 in.	8	2.18	$\geq 5.80+0.96\sigma$	NA	8	2.90	$\geq 3.63+0.96\sigma$	NA
25.6 to 29.5 in.	5	2.18	$\geq 5.80+0.83\sigma$	NA	5	2.90	$\geq 3.63+0.83\sigma$	NA

\*If Avg.  $E_{v2}$  criteria is not met ( $\sigma$  = standard deviation of measurements based on  $N$  number of tests)

**Table 3. Summary of target  $E_{v2}$  and  $E_{v2}/E_{v1}$  ratio values per (ATB Vag 2005) – Metric units.**

Depth below surface of base layer (mm)	Asphalt Pavement				Concrete Pavement			
	N	Min. $E_{v2}$ (MPa)	Avg. $E_{v2}$ (MPa)	Ratio* $E_{v2}/E_{v1}$	N	Min. $E_{v2}$ (MPa)	Avg. $E_{v2}$ (MPa)	Ratio* $E_{v2}/E_{v1}$
0-250 mm	8	125	$\geq 140 + 0.96\sigma$	$\leq 2.8$	8	105	$\geq 120 + 0.96\sigma$	$\leq 2.8$
0-250 mm	5	125	$\geq 140 + 0.83\sigma$	$\leq 1 + 0.013E_{v2}$	5	105	$\geq 120 + 0.83\sigma$	$\leq 1 + 0.015E_{v2}$
251-500 mm	8	32	$\geq 40 + 0.96\sigma$	$\leq 2.8$	8	45	$\geq 55 + 0.96\sigma$	$\leq 3.5$
251-500 mm	5	32	$\geq 40 + 0.83\sigma$	$\leq 1 + 0.063E_{v2}$	5	45	$\geq 55 + 0.83\sigma$	$\leq 1 + 0.046E_{v2}$
501-550 mm	8	32	$\geq 40 + 0.96\sigma$	NA	8	45	$\geq 55 + 0.96\sigma$	NA
501-550 mm	5	32	$\geq 40 + 0.83\sigma$	NA	5	45	$\geq 55 + 0.83\sigma$	NA
551-650 mm	8	20	$\geq 30 + 0.96\sigma$	NA	8	30	$\geq 35 + 0.96\sigma$	NA
551-650 mm	5	20	$\geq 30 + 0.83\sigma$	NA	5	30	$\geq 35 + 0.83\sigma$	NA
651-750 mm	8	15	$\geq 20 + 0.96\sigma$	NA	8	20	$\geq 25 + 0.96\sigma$	NA
651-750 mm	5	15	$\geq 20 + 0.83\sigma$	NA	5	20	$\geq 25 + 0.83\sigma$	NA

\*If Avg.  $E_{v2}$  criteria is not met ( $\sigma$  = standard deviation of measurements based on  $N$  number of tests)

### 2.1.5 Modulus of Subgrade Reaction Testing

A static plate load test was conducted in accordance with AASHTO T222-81 (2012) to determine  $k$  value using a 30 in. diameter loading plate setup shown in Figure 5. The applied stress was increased up to 30 psi in 5 psi increments, by monitoring the corresponding plate deformation readings at three locations along the edge of the plate. The uncorrected  $k$  value was determined using Eq. 14.

$$k'_u = \frac{10 \text{ psi}}{\delta_o} \quad (14)$$

where,  $k'_u$  = uncorrected modulus of subgrade reaction (pci),  $\delta_o$  = deformation corresponding to the 10 psi loading increment (inches). In this study, a 10 psi loading increment over the corrected linear portion of the loading curve and the deformation measured for that loading increment are used for calculation. The  $k'_u$  value is then corrected for plate bending to determine  $k_u$  following the procedure described in the test standard and Eq. 16 for  $k'_u \geq 100$  pci and  $\leq 1000$  pci.

$$k_u = 19170 - \frac{19154}{(1 + 0.0009 \times k'_u)^{0.05188}} \quad (15)$$



**Figure 5. APLT test setup with 30 in. diameter plate for AASHTO T222 static plate load test (note: wheels not in contact with ground during testing).**

#### 2.1.6 Confining Stress-Dependent Resilient Modulus Test

A controlled confining stress-dependent resilient modulus test was conducted using an 8 in. diameter loading plate. The full test sequence involves one conditioning sequence of 500 cycles followed by 15 loading sequences with 100 cycles each, similar to AASHTO T307 (2000) laboratory test procedure. A 30 second rest period is used between each loading sequence. An example test sequence is provided in Table 4 and the setup is shown in Figure 6. Results from this testing were used to develop a stress-dependent constitutive model to predict  $M_r$  as shown in Eq. (16):

$$M'_{r,\sigma} = s_1 (\sigma_{\max})^{s_2} (\sigma_{sc})^{s_3} \quad (16)$$

where,  $M'_{r,\sigma}$  = stress-dependent resilient modulus corrected for plate size;  $\sigma_{\max}$  = maximum applied plate contact stress;  $\sigma_{sc}$  = surface confining stress; and  $s_1$ ,  $s_2$ , and  $s_3$  = regression constants.

**Table 4. Example confining stress-dependent resilient modulus test sequence.**

Load Sequence	Maximum plate Stress ( $\sigma_{max}$ ), psi	Maximum surface confining stress ( $\sigma_{sc}$ ), psi	Cycles
Conditioning	30	15	500
1	6	3	100
2	9	3	100
3	12	3	100
4	10	5	100
5	15	5	100
6	20	5	100
7	20	10	100
8	30	10	100
9	40	10	100
10	25	15	100
11	30	15	100
12	45	15	100
13	35	20	100
14	40	20.0	100
15	60	20.0	100

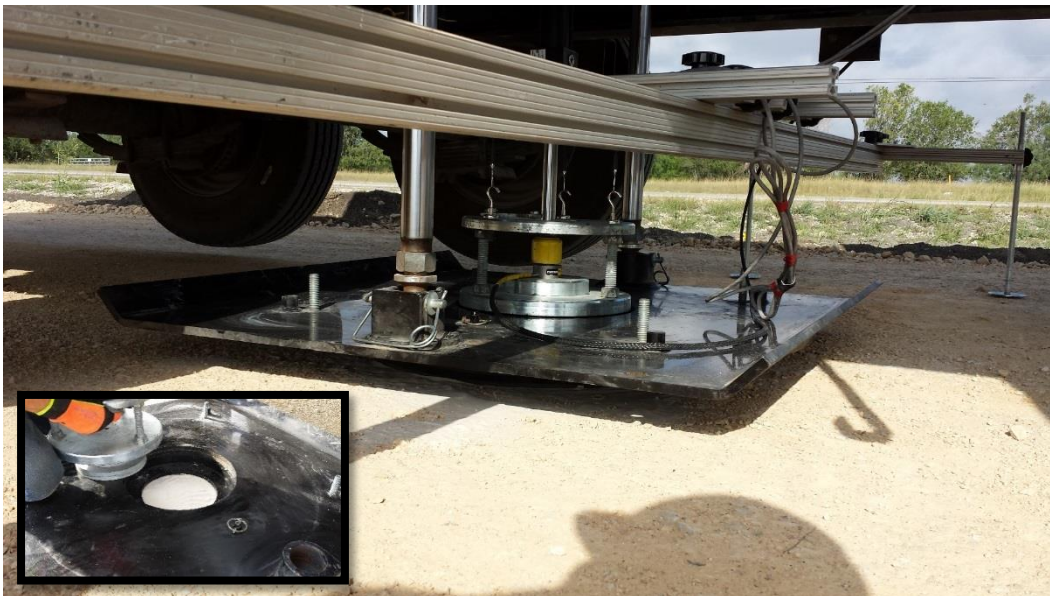


**Figure 6. APLT test setup with a confining plate and a 8 in. diameter loading plate.**

## 2.2 Dynamic Cone Penetration (DCP) Testing

DCP tests were performed in accordance with ASTM D6951-03 “Standard Test Method for Use of the Dynamic Cone Penetrometer in Shallow Pavement Applications”. The tests involved dropping a 17.6 lb hammer from a height of 22.6 in. and measuring the resulting penetration depth. A 30 in. penetrating rod was used. California bearing ratio (CBR) values were determined using Eqs. (17) and (18), whichever is appropriate, where the dynamic penetration index (*DPI*) is in units of mm/blow.

$$CBR(\%) = \frac{292}{DPI^{1.12}} \text{ for all materials except CL soils with } CBR < 10 \quad (17)$$

$$CBR(\%) = 1 / (0.017019 \times DPI)^2 \text{ for CL soils with } CBR < 10 \quad (18)$$

## 2.3 Laboratory Testing

Laboratory tests were performed on bulk samples of aggregate base materials obtained from the test section, to determine the soil gradation parameters and soil classification.

A soil grain-size analysis test was conducted in accordance with ASTM C136M-14 “Standard Test Method for Sieve Analysis of Fine and Coarse Aggregates”. Tests were conducted on oven-dried material. Material was first washed through the No. 200 sieve and the material retained on the No. 200 sieve was oven-dried and dry sieved.

The material was classified in accordance with ASTM D2487-11 “Standard Practice for Classification of Soils for Engineering Purposes (Unified Soil Classification System)” and ASTM D3282-09 “Standard Practice for Classification of Soils and Soil-Aggregate Mixtures for Highway Construction Purposes”.



### 3 Experimental Study

#### 3.1 Field Experimental Study

For this project, the field testing program involved a series of cyclic and static plate load tests. Table 5 provides details of the APLT configuration, load cycles, and cyclic stresses used in this study.

**Table 5. Summary of plate tests and configurations.**

Test Designation	Number of Load Cycles	Target Stress Range (psi)		Plate Configuration/Notes
		Min	Max	
A	1000 and 10,000	2	50	12 in. diameter, flat plate including deflection readings @ 2r and 3r.
B-1	2	0	Stress to reach 0.2 inch def.	Static Test, 12 in. diameter, flat plate, load applied in six increments per DIN 18134 (2001)
B-2	2	0	72.5	Static Test, 12 in. diameter, flat plate, load applied in six increments per DIN 18134 (2001)
C	2	0	30	30 in. diameter, flat plate, in 5 psi increments per AASHTO T222
D	2000	3	60	8 in. diameter, flat plate w/ 24 in. confining plate.

The roadway sections in this study contained geogrid between the aggregate surface layer and the underlying untreated subgrade. Table 6 identifies the geogrid used in the field testing program.

**Table 6. Summary geogrid material mechanical properties.**

Geogrid	Type	Mechanical Properties
TX5	Multi-axial geogrid with hexagonal structure and triangular apertures	Rib pitch 40 mm (1.6 inch)

### 3.2 Project Details

Table 7 provides details for the project location and nominal profiles of the roadway test areas. Figure 7 shows the April 17, 2015 APLT test locations. The locations are based on an average of 2 Hz autonomous GPS measurements at each test location. A \*.kmz file that allows greater detail for viewing the test locations is provided separate from this report.

**Table 7. Summary of project location and notes.**

Site/Location	Notes
West Hunt Highway Between N. Mountain Vista Blvd & N. Village Lane San Tan Valley, AZ; Coordinates: 33°11.255'N, 111°35.730'W	Unpaved road with nominal 5 inches of aggregate base course over a CBR = 5 to 50 (decreasing w/depth) subgrade. TX5 placed at the subgrade/base interface. To be paved with HMA (~Spring 2015).



**Figure 7. APLT test locations on April 17, 2015 testing between N. Mountain Vista Blvd & N. Village Lane in San Tan Valley, AZ.**

Figure 8 shows the aggregate base course material placed over TX5 geogrid. Figure 9 shows the pneumatic roller used for compaction of the aggregate base layer. The APLT test setup is shown in Figure 10.

Pictures of the loose material used in particle-size analysis and gravel size material (coarser than No. 4 sieve) are shown in Figure 11. Particle-size analysis results of the base material is provided in Figure 12 with reference to the DOT gradation specification (see MAG (2013) Standard Specifications Section 310).

The material consists of a maximum particle size of 1.5 in. with about 5.7% passing the No. 200 sieve, and is classified as poorly-graded gravel with sand and silt (GP-GM) according to the USCS classification and A-1-a according to the AASHTO classification. The material included rounded to sub-rounded gravel particles with some fractured gravel.



**Figure 8. Aggregate base course over TX5 (April 17, 2015).**





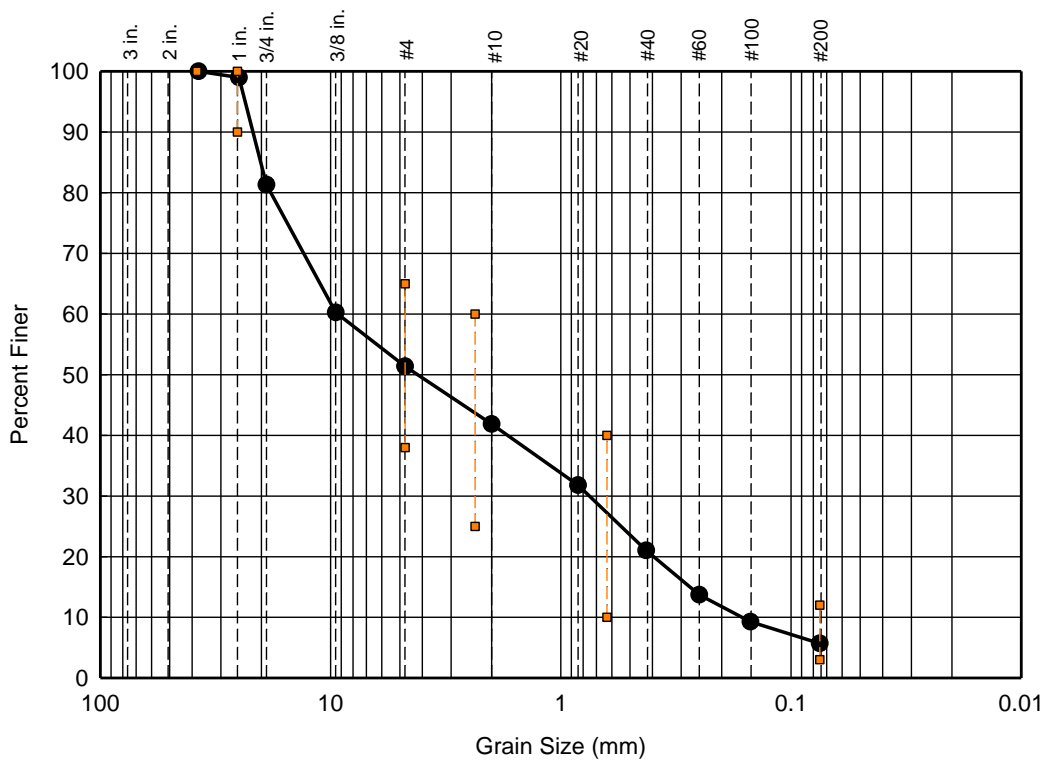
**Figure 9. Pneumatic tired roller used just prior to testing (April 17, 2015).**



**Figure 10. APLT testing at 30 in. static test point (April 17, 2015).**



**Figure 11. (top) Full gradation sample and (bottom) aggregate base course retained on No. 4 sieve after washing and oven-drying (April 17, 2015 sample).**



% Gravel		% Sand			% Fines
Coarse	Fine	Coarse	Medium	Fine	Silt + Clay
18.7	29.9	9.5	20.8	15.3	5.7

Gradation Parameters						
D <sub>10</sub> = 0.167	D <sub>30</sub> = 0.772	D <sub>50</sub> = 4.349	D <sub>60</sub> = 9.359	D <sub>85</sub> = 20.249	c <sub>u</sub> = 56.193	c <sub>c</sub> = 0.382

Atterberg Limits			Classification	
PL = NP	LL = NP	PI = NP	USCS = GP-GM Poorly graded gravel with sand and silt	AASHTO = A-1-a

**Figure 12. Grain-size analysis and classification of aggregate base course material with limits shown for MAG (2013) Standard Specification Section 310 (sampled April 17, 2015).**



## 4 Results

### 4.1 Dynamic Cone Penetration (DCP) Test Results

Figure 13 shows the CBR and cumulative blows profiles at all test locations. The CBR profiles show increasing CBR from about 10 to 50 with depth through the aggregate base course layer and then a reduction in CBR through the subgrade layer. The increase in CBR with depth in the aggregate base course is attributed to the effect of increasing confinement with depth. The subgrade profile shows that CBR decreases with depth from about 50% to 10%.

The aggregate base layer thickness was measured by excavating the base material down to the geogrid. The base layer thickness varied from 4.3 to 6.3 in. with an average thickness of 5.4 inches.

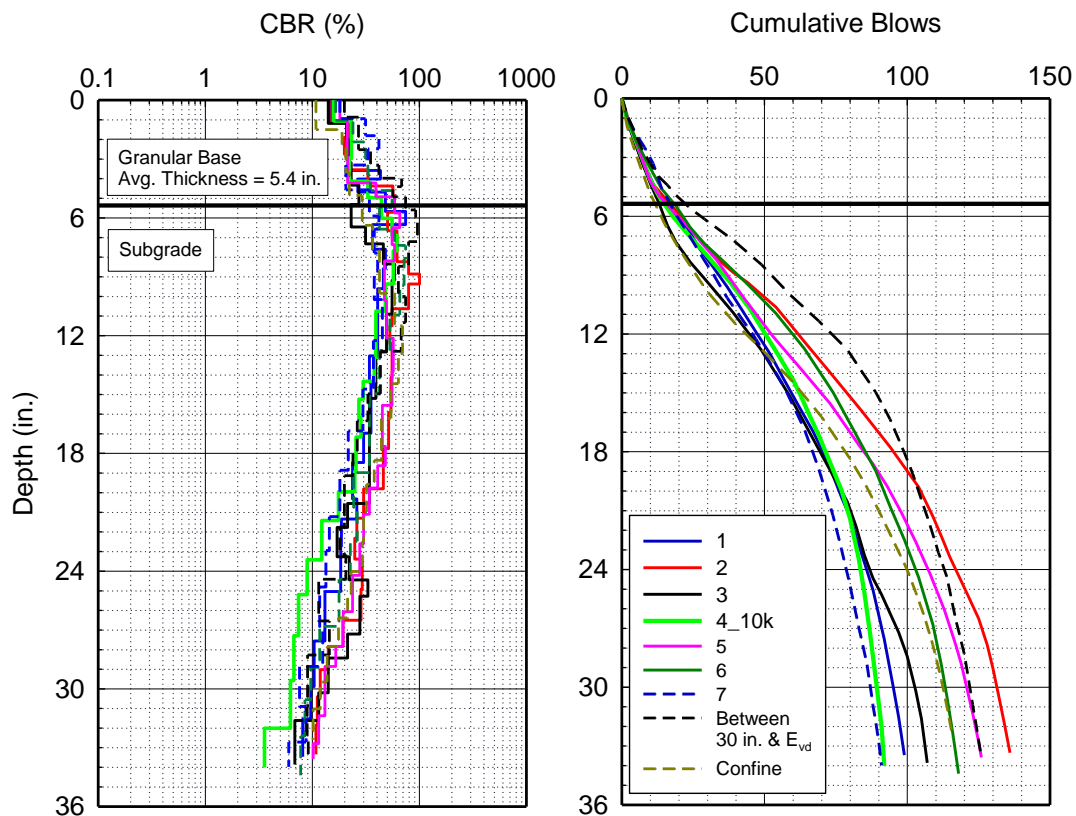


Figure 13. DCP profiles for all test locations.

## 4.2 In-Situ Composite Resilient Modulus

Table 8 summarizes the in-situ composite  $M_r$  and permanent deformation ( $\delta_p$ ) results from cyclic plate load tests (1,000 cycles each) performed at seven test locations. Individual layer aggregate base and subgrade layer  $r$  values are discussed in the next section. The in-situ composite  $M_r$  was calculated as the average of the last 50 loading cycles.

The in-situ average composite  $M_r$  was about 34 ksi and ranged between 26 and 42 ksi. The average permanent deformation at the end of 1,000 cycles was about 0.0590 inches and ranged between 0.0293 and 0.0846 inches for all tests.

Figure 14 summarizes the roadway sections in terms of the aggregate base layer thicknesses and average subgrade CBR to a depth of 12 in. below the bottom of the aggregate layer. In-situ composite  $M_r$  and  $\delta_p$  values at each test point are also summarized in Figure 14.

**Table 8. Comparison of test results for in-situ  $M_r$  and permanent deformation April 17, 2015 in-situ testing.**

Test Point	$M_r$ (psi) (cycles 950-1000)	$M_r$ (Base) (psi) (cycles 950-1000)	$M_r$ (sg) (psi) (cycles 950-1000)	$M_r$ (Base) / $M_r$ (sg) at 1,000 cycles	$\delta_p$ (in.)	$h_e/r$
1	26,294	236,821	9,743	24.3	0.0617	2.3
2	35,720	42,958	29,003	1.5	0.0593	1.0
3	35,320	133,011	17,231	7.7	0.0846	1.7
4	33,924	219,944	12,504	17.6	0.0572	2.3
5	42,441	—*	—*	—*	0.0293	0.7
6	34,192	—*	—*	—*	0.0562	0.7
7	31,865	145,735	12,238	11.9	0.0646	2.2
Min.	26,294	42,958	9,743	1.2	0.0293	0.7
Max.	42,441	236,821	29,003	21.0	0.0846	2.2
Avg.	34,251	155,694	16,144	11.0	0.0590	1.6

\*  $h_e/r < 1.0$  therefore not compliant with Odemark's MET analysis;  $h_e$  per Eq. 7.  
note: sensor at 3r used for layered analysis



As-built gravel layer thickness (in.)	1 5.0	2 5.5	3 5.6	4 5.7	5 5.2
Average Base CBR (%)*	24	29	21	26	25
Average Subgrade CBR (%) (12 in.)	42	61	42	42	53
In-Situ $M_r$ (psi)	26,294	35,720	35,320	33,924	42,441
Permanent Deformation, $\delta_p$ (in.)	0.0617	0.0593	0.0846	0.0572	0.0293
As-built gravel layer thickness (in.)	6 5.9	7 6.3	$E_v$ 4.3	8in. Confine 4.8	
Average Base CBR (%)*	32	30	32	18	
Average Subgrade CBR (%) (12 in.)	51	36	65	50	
In-Situ $M_r$ (psi)	34,192	31,865	—	$f(\sigma_{max}, \sigma_{sc})$	
Permanent Deformation, $\delta_p$ (in.)	0.0562	0.0646	0.0199	—	

\* DCP tests unconfined at surface; CBR profiles show increasing strength with depth.

**Figure 14. Summary of aggregate layer thicknesses and in-situ measurement values.**

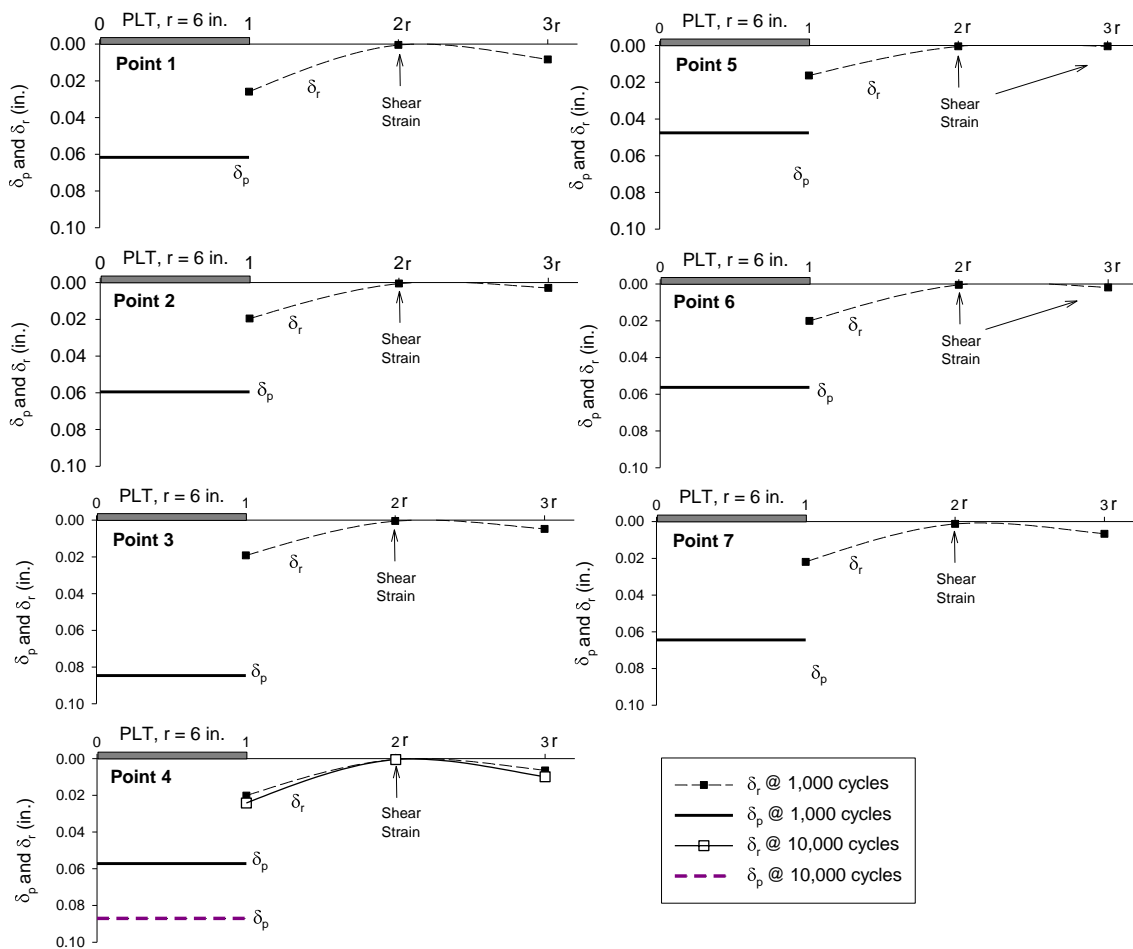
### 4.3 Two-Layer In-situ Resilient Modulus

APLT layer analysis tests were performed to measure deflections outside the 12 inch diameter plate to enable calculation of layer modulus values for both the aggregate base and subgrade. This analysis is helpful to better understanding and quantifying the influence of the geogrid in the stabilized aggregate layer.

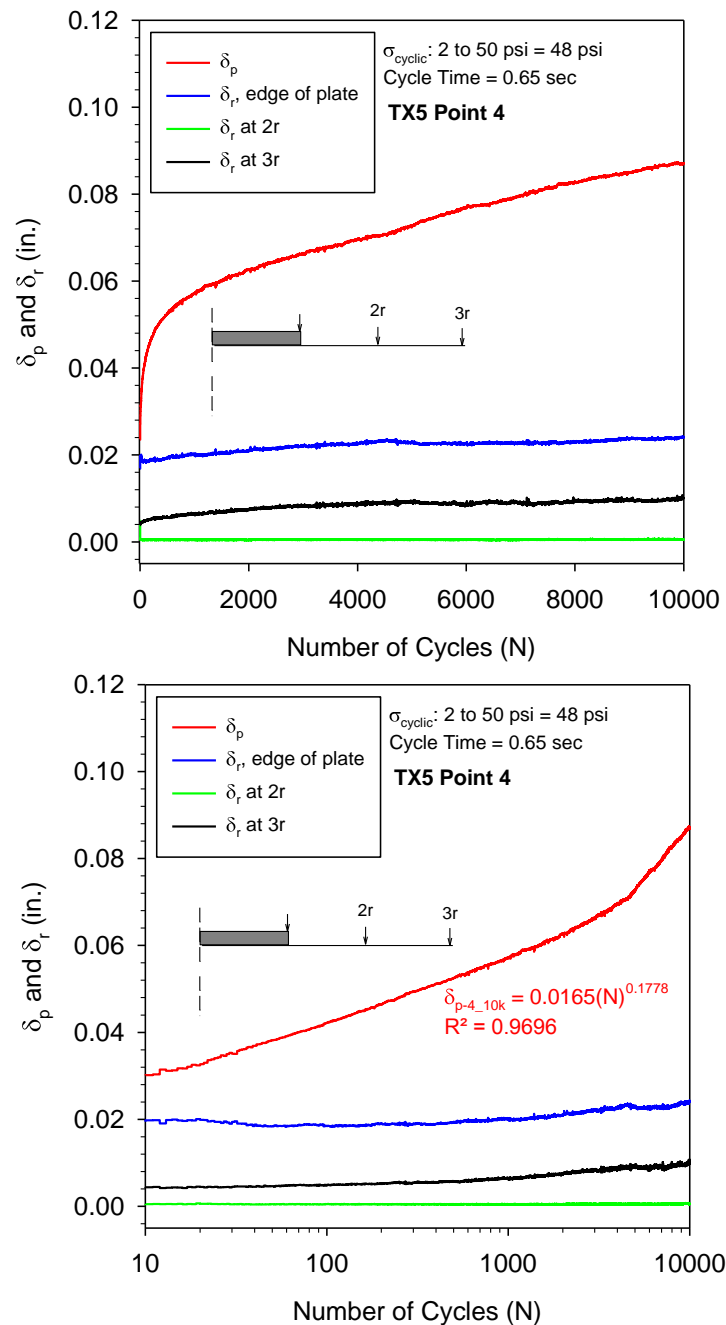
Based on the last 50 load cycles, Table 8 summarizes the aggregate base and subgrade layer modulus values. The calculated average modulus of the stabilized aggregate base layer was about 156 ksi, while the subgrade was about 16 ksi. Test points no. 5 and 6 resulted in  $h_e/r$  ratio  $< 1$  and were therefore not considered to meet the Odemark's analysis requirements (see section 2.1.2). Both of these test points resulted in very low 2r and 3r resilient deflections. Outside the perimeter of the load plate, it is expected that the unconfined aggregate dilated during testing.

Figure 16 shows the  $\delta_p$  of the plate, and resilient deflections ( $\delta_r$ ) at the edge of plate and at radial distances of 2r and 3r (where  $r = 6$  in.) with increasing load cycles for all test points. Figure 16 shows the 10,000 cycle tests results for permanent deformation and resilient deflections.

The results at all test locations show that the resilient deflections at 2r were less than at 3r, which is in contrast with the elastic theory, where the opposite is expected. Evidence of the 2r sensor showing less resilient deflection compared to the 3r sensors suggests cyclic shear strain induced volume change (i.e., dilation) in the stabilized aggregate outside of the perimeter of the loading plate. In well compacted granular materials, dilatancy often occurs under loading and is more pronounced at low stresses. It has been noted by Houston et al. (2008) that shear-induced dilatancy behavior of unsaturated materials at high suction results in greater tendency to dilate.



**Figure 15. Comparison of permanent plate deformation and resilient deflections at 1,000 at points 1 to 7 and 10,000 cycles at point 4.**



**Figure 16. Permanent plate deformation and resilient deflections measured at the edge of the plate and at  $2r$  and  $3r$  away from the plate center at test point 4 with 10,000 cycles.**

Figure 17 shows the calculated layer modulus values for each of the 10,000 cycles. As shown, the in-situ resilient modulus increased rapidly for the aggregate base layer for the first ~3000 cycles and then continued to increase at a slower rate. The rate of increase in modulus follows a logarithmic relationship with load cycles. The subgrade resilient modulus

decreased with increasing cycles. Based on a permanent deformation rate of 0.0001 in./cycle the transition from plastic deformation accumulation to near-linear elastic behavior ( $N^*$ , see section 4.7) occurs at 8,696 load cycles. At  $N^*$ , the in-situ  $M_{r(Base)}$  was about 321,881 psi (~2 times higher than the average resilient modulus from the 1,000 cycle tests).

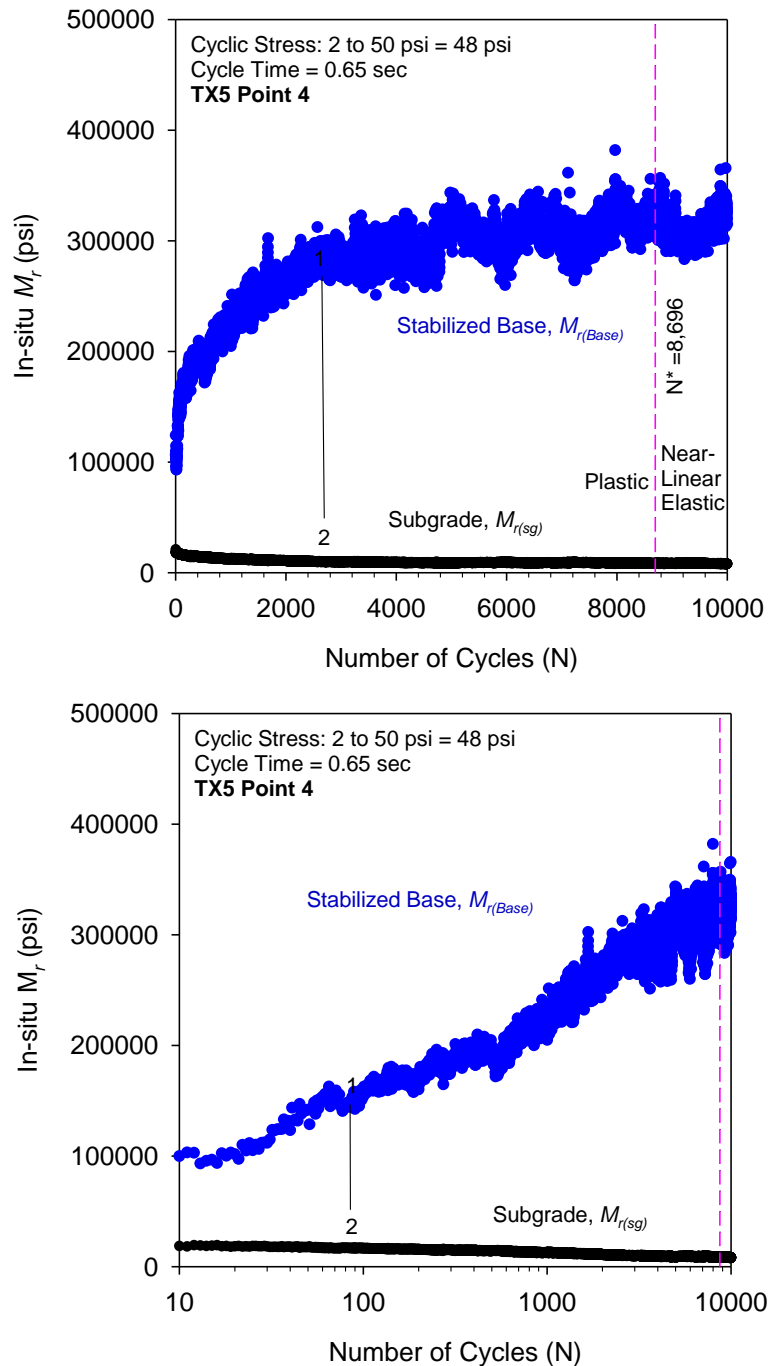


**Figure 17. In-situ  $M_r$  of base and subgrade layers from layered analysis versus number of cycles at test point 4 with 10,000 cycles.**

#### 4.4 $E_v$ Strain Modulus

Figure 18 shows the results of the  $E_v$  strain modulus test. The test was performed up to a maximum stress level of 72.5 psi, per the test requirement. Results show that the  $E_v$  results are stress range dependent, as expected. Relative to the target values provided in Table 1, 2, and 3 the  $E_v$  values and ratio meet or exceed minimum specified values in Europe for top of base.

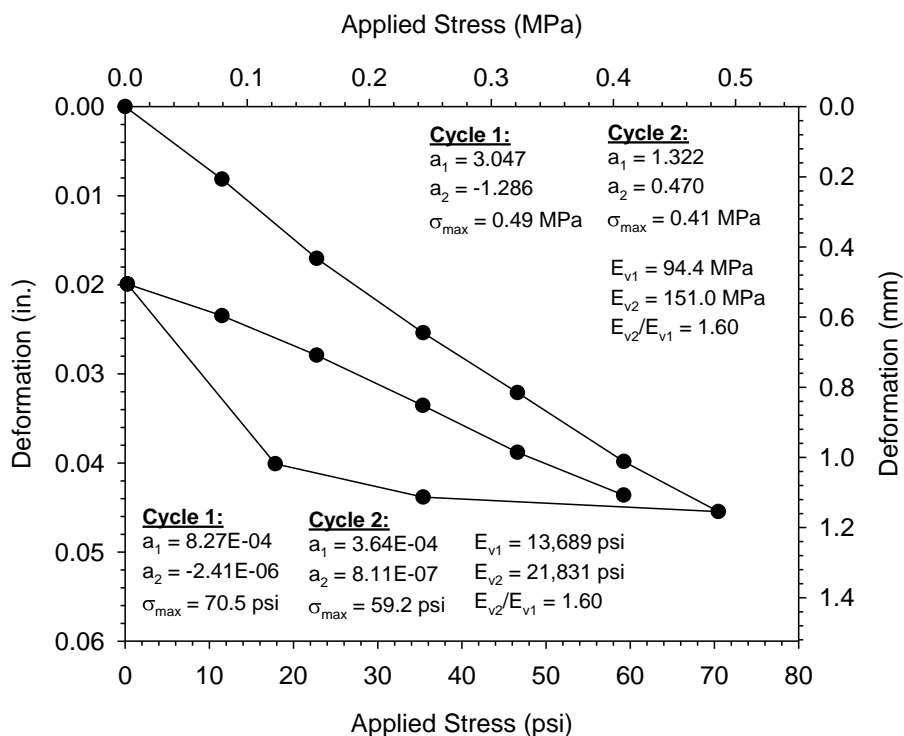


**Figure 18.  $E_v$  strain modulus applied stress versus settlement for TX5 section.**

#### 4.5 Modulus of Subgrade Reaction, $k$ -value

Figure 19 shows the results of the 30 in. diameter static plate load test. This test was performed next to the  $E_v$  test location. Based on the corrected stress deformation plot, the modulus of subgrade reaction,  $k$ -value, is 392 pci.

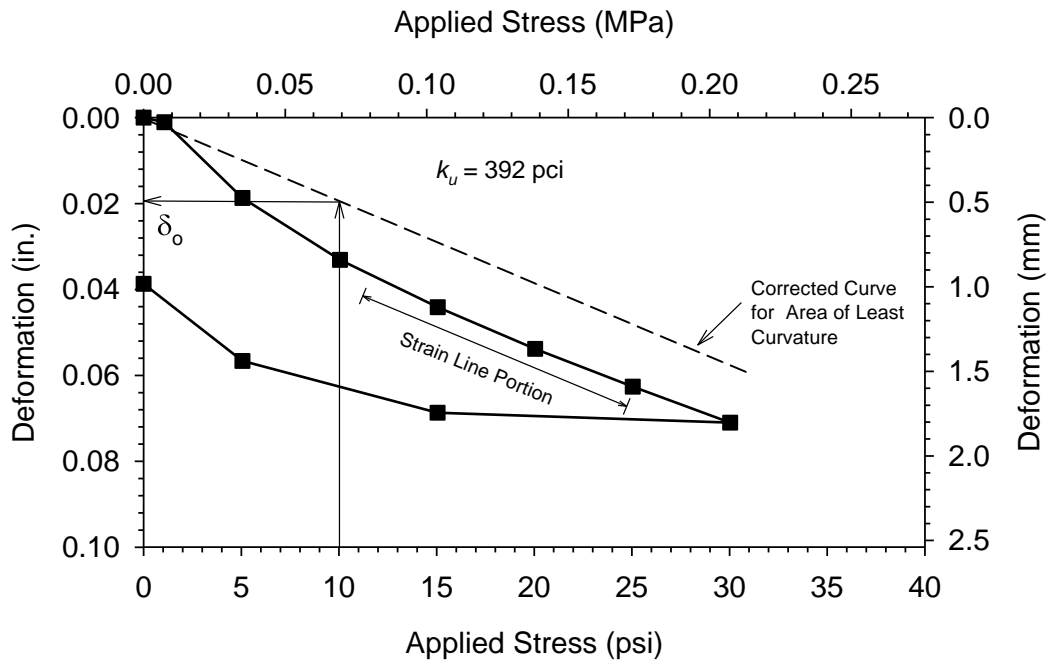


**Figure 19. k-value modulus of subgrade reaction for 30 in. diameter static plate load test for TX5 section.**

#### 4.6 In-situ Confining Stress Dependent Modulus

Figure 20 shows the results of the cyclic and confining stress dependent plate load test. Based on the model parameters, estimates of the composite in-situ resilient modulus can be made for the desired surface confining stress and maximum cyclic stress. For reference, 1 psi surface confinement with 15 psi maximum cyclic stress results in  $M'_{r,\sigma} = 69,207$  psi. The model shows that as the maximum cyclic stress decreases, the in-situ resilient modulus increases. This finding is confirmed by previous experience with testing stabilized aggregate base.

Figure 20 also shows the corresponding permanent deformations for the conditioning and 15 cyclic load steps. The results show that at higher cyclic stress values, the permanent deformation was still increasing after 100 cycles.

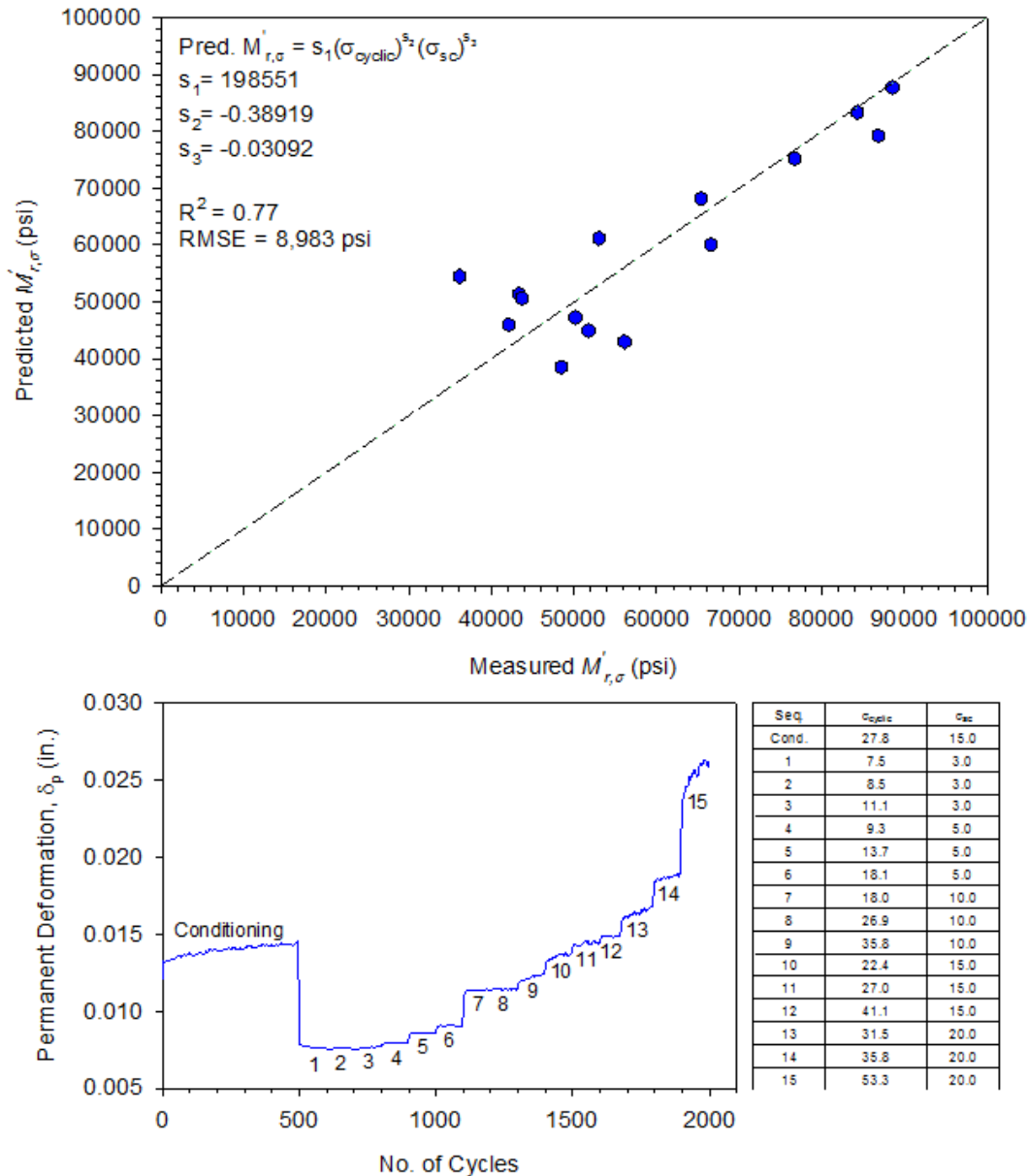


**Figure 20. In-situ  $M'_{r,\sigma}$  model and permanent deformation results for TX5 section.**

#### 4.7 Predicting Trafficking Performance

For all 1,000 cycle tests, the stresses were cycled between 2 psi and 50 psi with a nominal cyclic stress of 48 psi, the cycle times were 0.65 sec. (0.15 sec. load pulse + 0.45 sec. dwell time). In Figure 21, the permanent deformation versus number of load cycles is plotted. Table 9 summarizes the plastic deformation model parameters and comparisons between forecasted numbers of cycles ( $N^*$ ) and  $\delta_p$  to achieve the  $\delta_p$  rate limit (0.0001

in./cycle). Here  $N^*$  represents the cycle number at which the application of additional cyclic loadings results in very low accumulation of additional permanent deflection and the composite foundation layers are producing a resilient response.  $\delta_p$  at  $N^*$  is the permanent deformation often referred to as the post-compaction deformation. At  $N^*$  cycles and the associated permanent deformation, a stable equilibrium response from loading is anticipated (e.g., Collins et al. 1993).

Observation of the permanent deformation versus cyclic numbers for the 10,000 cycle test (Figure 16) shows that the deformation rate increases near-linearly with increasing load cycles. Plotted on a log-scale, this produces a slightly upward trending curve. Previous experience with 10,000 cycle testing with more well-graded aggregates at other sites indicate permanent deformation plots that are less linear (more asymptotic). Werkmeister et al. (2014) noted that permanent deformation behavior that produces a near-linear response is presumably linked to friction characteristics of the aggregate particles and number of grain contacts, where well-graded material is preferred.

**Table 9. Summary of permanent deformation prediction parameters**

Test Point	$C$	$d$	$R^2$	$N^*$ at $\Delta\delta_p =$ <b>0.0001</b> in./cycles	$\delta_p$ (in.) at $N^*$
1	0.0333	0.0905	0.9946	1,782	0.066
2	0.0373	0.0701	0.9827	1,149	0.061
3	0.0452	0.0922	0.9917	1,844	0.090
5	0.0988	0.0241	0.9696	2,104	0.069
6	0.0222	0.1334	0.9975	4,039	0.051
7	0.0406	0.0684	0.9814	1,105	0.067
4_10k	0.0165	0.1778	0.9696	8,696	0.066



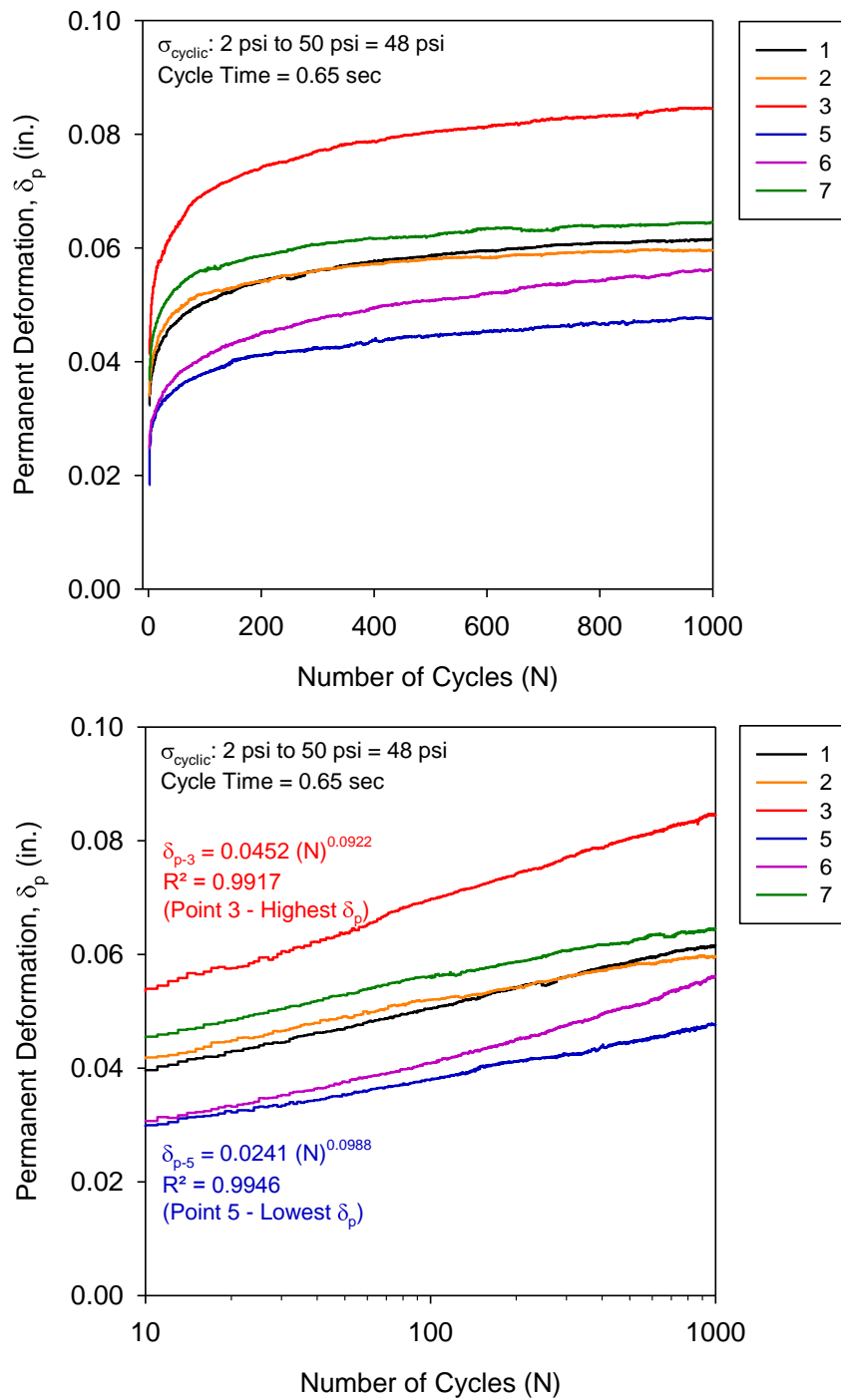
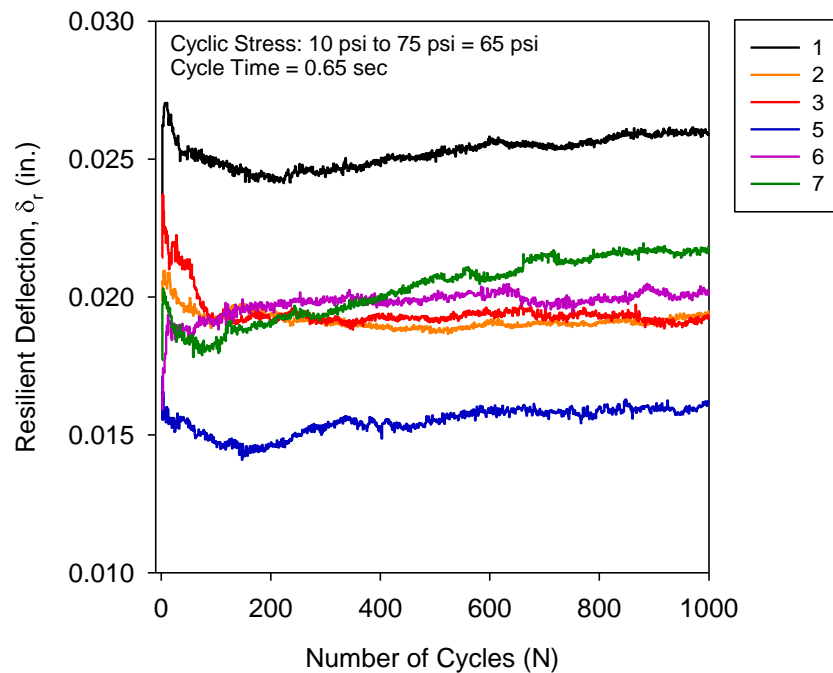


**Figure 21. Permanent deformation versus load cycle number at all test points.**

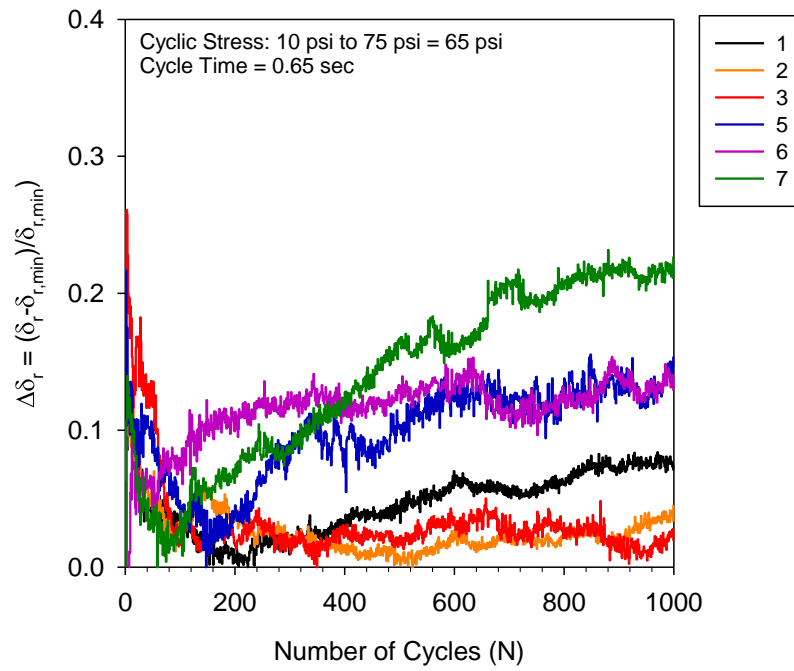
## 4.8 Additional Findings

Figure 22 shows the resilient deflection as a function of the number of load cycles for the 12 inch diameter plate testing. It was observed that the resilient deflection trends with increasing number of load cycles. For most plots, the TX5 test points produced a gradual decrease in resilient deflection followed by a gradual increase. The resilient deflections are normalized with the minimum resilient deflection as presented in Figure 23. Examining the results this way suggest that the stabilization mechanics of the geogrid may be increasing the resiliency as the permanent deformations (plastic strain, compaction, and consolidation) are reduced with each cycle.

The mechanics for this behavior warrants further investigation, but may be linked to stored energy in the geogrid by transferring shear strain in the aggregate to the geogrid.



**Figure 22. Resilient deflection versus load cycle number for all test points.**



**Figure 23. Change in resilient deflection (relative to the minimum resilient deflection) versus load cycle number for all test points.**

## 5 Conclusions and Recommendations

A summary of the key observations from the tests conducted in this study are as follows:

1. The road section selected for in-situ performance assessment provided an excellent opportunity to evaluate aggregate base course stabilized with TX5 geogrid. The aggregate base course classified as poorly-graded gravel with sand and silt (GP-GM) with 5.7% fines content.
2. For the 1,000 cycle tests, results showed that the in-situ composite resilient modulus in the TX5 geogrid stabilized section was about 34,251 psi at 48psi cyclic stress. The layered analysis in-situ resilient modulus averaged 155,694 psi for the aggregate base layer and 16,144 psi for the subgrade layer.
3. For the 10,000 cycle test, the in-situ resilient modulus rapidly increased in the aggregate base layer for the first ~3000 cycles and then continued to increase at a slower rate. Based on a permanent deformation rate of 0.0001 in./cycle the transition from plastic deformation accumulation to near-linear elastic occurs at  $N^* = 8,696$  cycles. At  $N^*$ , the in-situ  $M_r$  was about 321,881 psi (2x higher than the average value from the 1000 cycle tests).
4.  $E_v$  static plate test yielded  $E_{v1}$  of 13,689 psi with  $E_{v2}/E_{v1}$  ratio of 1.60.
5. Modulus of subgrade reaction,  $k_u$ , was 392 pci as measured from the 30 in. diameter plate.
6. Permanent deformation rate was observed to increase near-linearly with increasing load cycles for some of the 1,000 cycle tests and the 10,000 cycle test. Previous experience with 10,000 cycle testing with more well-graded aggregates at other sites indicate permanent deformation plots that are less linear (more asymptotic). This near-linear trend is presumably linked to friction characteristics of the aggregate particles and number of grain contacts, where well-graded material is preferred.
7. Based on the model parameters determined from the cyclic confining stress-dependent resilient modulus test, estimates of the composite in-situ resilient modulus can be made for the desired surface confining stress and maximum cyclic stress. For reference, 1 psi surface confinement with 15 psi maximum cyclic stress results in  $M'_{r,\sigma} = 69,207$  psi. The model shows that as the maximum cyclic stress decreases, the in-situ resilient modulus increases.

8. Observation of the resilient deflections with loading cycles shows that the TX5 becomes more resilient with increasing loading cycles beyond about 100 cycles.

---

## References

- AASHTO T307-99 (2000). "Standard Method of Test for Determining the Resilient Modulus of Soils and Aggregate Materials", Standard Specifications for Transportation Materials and Methods of Sampling and Testing, Twentieth Edition, American Association of State Highway and Transportation Officials, Washington, DC.
- AASHTO T222-81 (2012). "Standard Method of Test for Nonrepetitive Static Plate Load Test of Soils and Flexible Pavement Components for Use in Evaluation and Design of Airport and Highway Pavements", Standard Specifications for Transportation Materials and Methods of Sampling and Testing, Thirty Second Edition, American Association of State Highway and Transportation Officials, Washington, DC.
- AASHTO (1993). *AASHTO Guide for Design of Pavement Structures*, Published by the American Association of State Highway and Transportation Officials, Washington, D.C.
- Brown, S., and Hyde, A. (1975). "Significance of cyclic confining stress in repeated-load triaxial testing of granular material." *Transportation Research Record*, (537).
- Collins, I.F., Wang, A. P. and Saunders, L.R. (1993). Shakedown theory and the desing of unbound pavements. *Road and Transport Research*, Vol. 2, No. 4, Dec. pp. 28-39.
- DIN 18134. (2001). "Determining the deformation and strength characteristics of soil by the plate loading test," Technical Committee 05.03.00 Baugrund, Versuche und Versuchsgeräte of the Normenausschuss Bauwesen (Building and Civil Engineering Standards Committee).
- Houston, S. L., Perez-Garcia, N., and Houston, W., N. (2008). "Shear strength and shear-induced volume change behavior of unsaturated soils from triaxial test program." *Journal of Geotechnical and Geoenvironmental Engineering*, Vol. 134, No. 11, p. 1619-1632.
- Kim, K., Lee, S., Park, Y., Kim, S. (2012). "Evaluation of Size Effects of Shallow Foundation Settlement Using Large Scale Plate Load Test," *Journal of Korean Geotechnical Society*, 28(7), 67-75.

- 
- LeKarp, F., Isacsson, U., and Dawson, A. (2000). "State of the art. I: Resilient response of unbound aggregates." *Journal of Transportation Engineering*, American Society of Civil Engineers.
- Li, D., and Selig, E. T., (1994). Resilient modulus for fine-grained subgrade soils." *J. Geotech. Engrg.*, ASCE, 120(6), 939-957.
- MAG. (2013). *Uniform Standard Specifications for Public Works Construction, 2013* Revision to the 2012 Edition, Sponsored and Distributed by Maricopa Association of Governments (MAG), Phoenix, AZ.
- McMahon, T. F., and E.J. Yoder, (1960). "Design of a pressure sensitive cell and model studies of pressures on a flexible pavement subgrade." Proceedings, *Highway Research Board*, Vol. 39, pp. 650-682.
- Monismith, C.L., Ogawa, N., and Freeme, C. R. (1975). "Permanent deformation characteristics of subgrade soils due to repeated loading." *Transportation Research Record*, 537, 1-17.
- NCHRP. (2004). "Laboratory Determination of Resilient Modulus for Flexible Pavement Design," Research Results Digest Number 285, National Cooperative Highway Research Program, Transportation Research Board, Washington, D.C.
- Sowers, G. F., and A. B. Vesic. (1961). "Stress distribution beneath pavements of different rigidities." Proceedings, *International Conference on Soils Mechanics and Foundation Engineering*, 5<sup>th</sup>, vol. 2, pp. 327-332
- Ullidtz, P. (1987). *Pavement Analysis*, Elsevier, New York, NY.
- Werkmeister, S., Dawson, A., and Wellner, F. (2013). "Permanent deformation behavior of granular materials and the shakedown concept." Transportation Research Record, No. 1757, *Journal of the Transportation Research Board*, p. 75-81
- White, D. J. (2015). "Field Evaluation of Plate Size Corrections for Cyclic Plate Load Testing: Geogrid Stabilized Aggregate Base over Soft Subgrade," *Interim Report*, Ingios Geotechnics, Inc. Boone, Iowa USA